

Noyori Hydrogenation: Aromaticity, Synchronicity, and Activation Strain Analysis

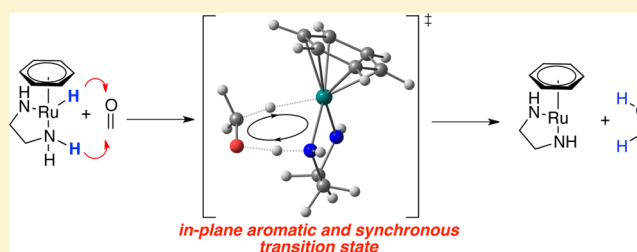
Olalla Nieto Faza,[†] Carlos Silva López,[†] and Israel Fernández^{*‡}

[†]Departamento de Química Orgánica, Universidade de Vigo, Lagoas-Marcosende s/n 36310, Vigo, Spain

[‡]Departamento de Química Orgánica, Facultad de Química, Universidad Complutense, 28040 Madrid, Spain

S Supporting Information

ABSTRACT: By means of density functional theory calculations, we have computationally explored the intimacies of the crucial step of Noyori hydrogenation reactions of multiple bonds. This process can be considered analogous to the so-called double group transfer reactions. Both kinds of transformations proceed concertedly via the simultaneous migration of two hydrogen atoms/groups in a pericyclic [$\sigma 2s + \sigma 2s + \pi 2s$] reaction through six-membered transition structures. Despite the structural resemblances of both types of saddle points, significant differences are found in terms of synchronicity and in-plane aromaticity. In addition, the activation strain model has been used to get quantitative insight into the factors which control the corresponding barrier heights. It is found that the presence of a heteroatom in the acceptor moiety is responsible for a remarkable increase of the interaction energy between the reactants which can compensate the destabilizing effect of the strain energy associated with the deformation of the initial reagents leading to low reaction barriers.



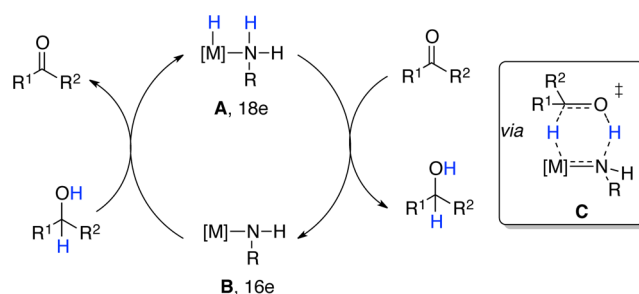
INTRODUCTION

The catalytic Noyori asymmetric hydrogenation (NAH) reaction constitutes one of the most useful reaction in organic chemistry. This process efficiently reduces multiple bonds (mainly polar double bonds, i.e., ketones, aldehydes, and imines) with high to complete enantioselectivity.¹ The importance of this reaction is clearly reflected in the good number of industrial processes that use this transformation to produce enantioenriched compounds in an environmentally benign manner without emitting waste or coproducts.²

Besides the synthetic applications of this reaction, the mechanism of the process has attracted much attention as well in view of the impressive number of experimental and computational studies focused on this transformation reported in the literature.³ Consensus has been reached that this reaction involves metal–ligand bifunctional catalysis, where both the transition metal and the surrounding ligand directly participate in the dehydrogenative and hydrogenative processes (Scheme 1). There is general agreement that the reduction of the double bond occurs in an outer coordination sphere of **A**, and therefore, it does not require any coordinative unsaturation at the transition metal. Therefore, the reactive species is a metal hydride (M–H) species, and the hydride delivery to the electrophilic carbon atom takes place via the six-membered pericyclic transition state **C**.³ Moreover, this step is crucial because the enantioselection of the process is suggested to occur in this pericyclic reaction.^{3a,h}

Interestingly, the six-membered transition state depicted in Scheme 1 structurally resembles that for double hydrogen atom-transfer reactions, a particular case of double group

Scheme 1



transfer (DGT) reactions where two hydrogen atoms migrate simultaneously from one compound to another in a concerted reaction pathway.^{4,5} These [$\sigma 2s + \sigma 2s + \pi 2s$] thermally allowed pericyclic transformations share a common feature: they proceed via a six-membered ring transition structure that is highly *in-plane* aromatic⁶ as indicated by the high negative nucleus independent chemical shifts (NICS) values⁷ computed at the (3,+1) ring critical point of the electron density⁸ (NICS ≈ -26 ppm).

Similar to other pericyclic processes such as [3 + 2] cycloadditions^{9,10} or Alder–ene reactions,¹¹ DGT reactions are associated with relatively high barriers despite the aromatic character of the corresponding transition states. This has been ascribed to the strong destabilizing effect of the strain associated with the structural rearrangement of the reactants

Received: April 18, 2013

Published: May 17, 2013

which cannot be compensated by the gain in stability through aromaticity in the transition structures.¹² For this reason, it has been suggested that this strain energy becomes the controlling factor for the high activation barriers of these transformations.^{12,13}

Due to the structural resemblances between the transition states associated with DGT reactions and those proposed for the crucial step of the Noyori hydrogenation, we were curious to compare both types of processes in terms of energetic, aromaticity, and synchronicity criteria. Therefore, we report herein the results of a density functional theory (DFT) study aimed at a deeper understanding of the effect of the metal fragment on the double hydrogen atom transfer occurring in the Noyori hydrogenation reaction.

THEORETICAL METHODS

Computational Details. All of the calculations reported in this paper were obtained with the GAUSSIAN 09 suite of programs.¹⁴ All reactants, transition structures, and reaction products were optimized using the hybrid functional B3LYP¹⁵ with double- ζ quality plus polarization def2-SVP basis sets¹⁶ for all atoms. Reactants and products were characterized by frequency calculations at the B3LYP/def2-SVP level and have positive definite Hessian matrices. Transition structures (TS's) show only one negative eigenvalue in their diagonalized force constant matrices, and their associated eigenvectors were confirmed to correspond to the motion along the reaction coordinate under consideration using the Intrinsic Reaction Coordinate (IRC) method.¹⁷ Single-point energy calculations were performed on the B3LYP/def2-SVP-optimized geometries using Truhlar's meta hybrid exchange-correlation functional M06¹⁸ with the triple- ζ quality plus polarization def2-TZVP basis sets.¹⁶

The aromatic character of the transition structures has been confirmed by the computation of the nucleus independent chemical shift (NICS) values computed at the (3,+1) ring critical point of the electron density (see below). This point was selected due its high sensitivity to diamagnetic effects and its unambiguous character.¹⁹ In addition, the more reliable NICS(1)_{zz} (out-of-plane component of the isotropic NICS tensor) values have been also computed. These calculations have been carried out using the gauge invariant atomic orbital (GIAO) method²⁰ at the B3LYP/def2-SVP level. This scheme is denoted GIAO-B3LYP/def2-SVP. In addition, the diatropic currents associated with the aromatic character of the transition states have been studied with the help of the anisotropy of the induced current density (ACID) method, developed by Herges and co-workers.²¹

The synchronicity^{22,23} of the reactions was quantified by using a previously described approach.²⁴ For a given concerted reaction, "synchronicity" is defined as²⁵

$$S_y = 1 - \frac{\sum_{i=1}^n \frac{|\delta B_i - \delta B_{AV}|}{\delta B_{AV}}}{2n - 2}$$

where n is the number of bonds directly involved in the reaction (in this case, $n = 6$) and δB_i stands for the relative variation of a given bond index B_i at the transition state (TS), according to the formula

$$\delta B_i = \frac{B_i^{TS} - B_i^R}{B_i^P - B_i^R}$$

where the superscripts R and P refer to the reactants and the product, respectively. The average value of δB_i , denoted as δB_{AV} , is therefore

$$\delta B_{AV} = n^{-1} \sum_{i=1}^n \delta B_i$$

The Wiberg bond indices²⁶ B_i were computed using the natural bond orbital (NBO)²⁷ method.

Activation Strain Analyses of Reaction Profiles. The relatively recent introduction of the so-called *activation strain model*²⁸ has allowed us to gain more insight into the physical factors which control how the activation barriers arise in different fundamental processes. This method is also known as the *distortion/interaction model*, as proposed by Houk and co-workers.⁹ The activation strain model is a fragment approach to understanding chemical reactions, in which the height of reaction barriers is described and understood in terms of the original reactants.²⁸ This method is a systematic extension of the fragment approach from equilibrium structures to transition structures as well as *nonstationary* points, e.g., points along a reaction coordinate. Thus, the potential energy surface $\Delta E(\zeta)$ is decomposed, along the reaction coordinate ζ , into the strain $\Delta E_{\text{strain}}(\zeta)$ associated with deforming the individual reactants plus the actual interaction $\Delta E_{\text{int}}(\zeta)$ between the deformed reactants:

$$\Delta E(\zeta) = \Delta E_{\text{strain}}(\zeta) + \Delta E_{\text{int}}(\zeta)$$

Here, the reaction coordinate is defined as the projection of the IRC on the forming C...H distance between the carbon atom of the multiple bond and the hydrogen atom transferred from the transition metal (Figure 1). This reaction coordinate ζ undergoes a well-defined change in the course of the reaction from ∞ to the equilibrium H...C distance in the corresponding transition structures.

The strain $\Delta E_{\text{strain}}(\zeta)$ is determined by the rigidity of the reactants and on the extent to which groups must reorganize in a particular reaction mechanism, whereas the interaction $\Delta E_{\text{int}}(\zeta)$ between the reactants depends on their electronic structure and on how they are mutually oriented as they

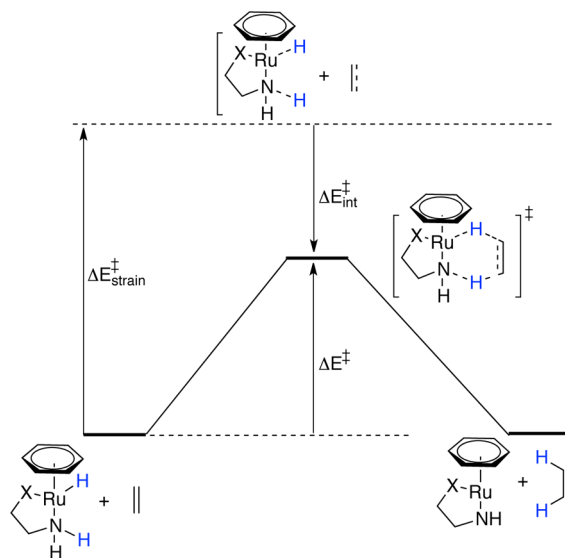
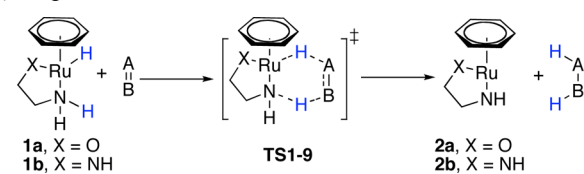
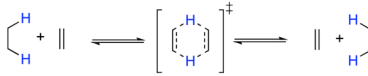
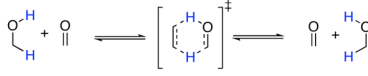


Figure 1. Illustration of the activation strain model for Noyori hydrogenation reaction.

Table 1. Free Activation Barriers and Reaction Energies^a (at 298 K, in kcal/mol), Synchronicities (S_y), and NICS Values (in ppm) of the Considered Noyori Hydrogenations



Entry	Reaction	ΔG_{298}^\ddagger	ΔG_R	S_y^b	NICS ^{b,c}
1	1a + H ₂ C=CH ₂ → 2a + H ₃ C-CH ₃	+27.8	-21.5	0.75	-16.0 (-19.7)
2	1a + HC≡CH → 2a + H ₂ C=CH ₂	+24.7	-30.9	0.65	-7.8 (-8.8)
3	1a + H ₂ C=O → 2a + H ₃ C-OH	+10.0	-6.5	0.79	-13.7 (-15.3)
4	1a + Me ₂ C=O → 2a + Me ₂ HC-OH	+18.5	+3.3	0.81	-13.7 (-13.5)
5	1a + H ₂ C=NH → 2a + H ₃ C-NH ₂	+19.0	-13.2	0.80	-12.9 (-15.6)
6	1b + H ₂ C=CH ₂ → 2b + H ₃ C-CH ₃	+28.5	-24.6	0.77	-16.1 (-20.6)
7	1b + HC≡CH → 2b + H ₂ C=CH ₂	+25.1	-34.0	0.67	-8.3 (-9.7)
8	1b + H ₂ C=O → 2b + H ₃ C-OH	+9.4	-9.6	0.74	-11.6 (-13.7)
9	1b + H ₂ C=NH → 2b + H ₃ C-NH ₂	+19.5	-16.3	0.83	-13.3 (-17.0)
10		+57.7	0.0	0.91	-27.8 (-36.1)
11		+36.2	0.0	0.91	-24.7 (-26.1)

^aComputed at the M06/def2-TZVP//B3LYP/def2-SVP level. ^bComputed at the B3LYP/def2-SVP level. ^cValues correspond to NICS values computed at the [3,+1] ring critical point of the electron density, whereas values in parentheses are the corresponding NICS(1)_{zz} values, computed one angstrom above the ring critical point.

approach each other. It is the interplay between $\Delta E_{\text{strain}}(\zeta)$ and $\Delta E_{\text{int}}(\zeta)$ that determines if and at which point along ζ a barrier arises. The activation energy of a reaction $\Delta E^\ddagger = \Delta E(\zeta^{\text{TS}})$ consists of the activation strain $\Delta E_{\text{strain}}^\ddagger = \Delta E_{\text{strain}}(\zeta^{\text{TS}})$ plus the TS interaction $\Delta E_{\text{int}}^\ddagger = \Delta E_{\text{int}}(\zeta^{\text{TS}})$ (see Figure 1):

$$\Delta E^\ddagger = \Delta E_{\text{strain}}^\ddagger + \Delta E_{\text{int}}^\ddagger$$

RESULTS AND DISCUSSION

Structures and Aromaticity. In Table 1, we provide an overview of the studied hydrogenation reactions computed at the M06/def2-TZVP//B3LYP/def2-SVP level together with the two archetypical DGT reactions, i.e., the double hydrogen atom migration from ethane to ethene and the Meerwein–Ponndorf–Verlay (MPV) reduction of formaldehyde by methanol previously reported by us.⁶ We have considered the model active ruthenium(II) catalysts **1a** and **1b** (also studied by Noyori and co-workers in their seminal computational study on the reduction of ketones using $[\text{RuCl}_2(\eta^6\text{-arene})]_2$ and a β -amino alcohol or 1,2-diamines)^{3a} as reducing agents of ethene and ethyne and the corresponding processes involving heteroatoms (formaldehyde, acetone, and methanimine).

Figure 2 shows the optimized geometries of selected transition structures associated with the above reactions. In all cases, the transformations occur via highly planar 6-membered ring transition states where the corresponding C–C, C–N, or C–O bond lengths are intermediate between double/triple and single/double bonds. This agrees well with the participation of the π -orbitals of the acceptor moiety in the migration of the $\sigma_{\text{H-Ru}}$ and $\sigma_{\text{H-N}}$ bonds expected for a pericyclic $[\sigma 2s + \sigma 2s + \pi 2s]$ process. Interestingly, the computed synchronicities (S_y , ranging from 0.65 to 0.83) indicate that the Noyori hydrogenations are more asynchronous than the related DGT reactions (which exhibit S_y values close to the perfect synchronicity). Nevertheless, the observed bond length equalizations and planarity of the cyclic transition states fulfill the so-called geometric aromaticity criterion,²⁹ therefore suggesting that these processes proceed via aromatic transition states. To check this hypothesis, we have calculated the corresponding NICS(0) values computed at the (3,+1) ring critical point of the electron density and the more reliable NICS(1)_{zz} values, computed 1 Å above this point. As readily seen in Table 1, the computed negative values (NICS(0) values ranging from -7.8 to -16.1 ppm and NICS(1)_{zz} values ranging

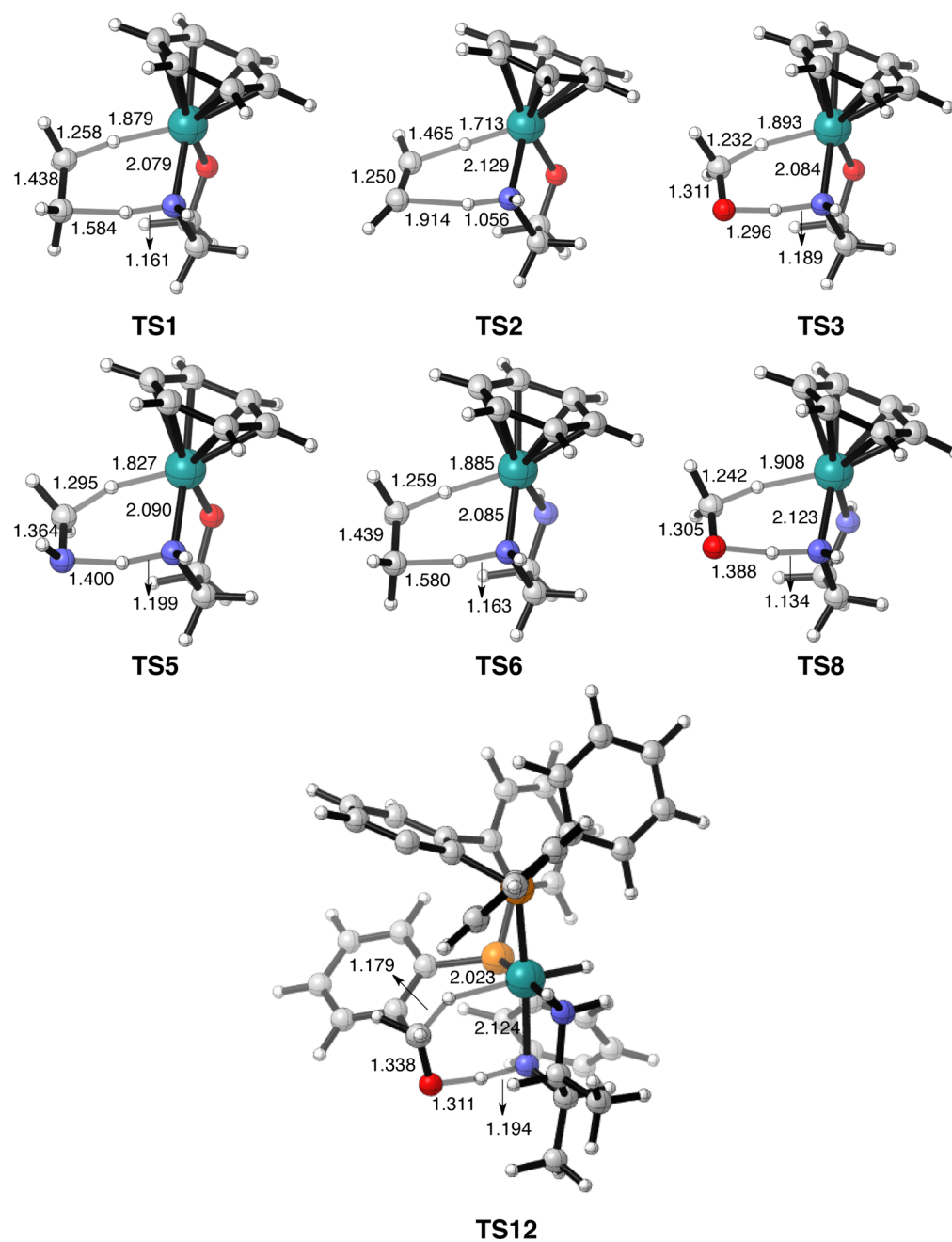


Figure 2. Optimized transition-state geometries (bond distances are given in Å), computed at the B3LYP/def2-SVP level.

Scheme 2



from -8.8 to -20.6 ppm) clearly confirm the aromatic nature of these saddle points and indicate that these species are less aromatic than the transition states associated with the analogous DGT reactions (see Table 1, entries 10 and 11). Therefore, it can be concluded that the Ru(II)–Noyori hydrogenations occur concertedly through transition structures

which are less synchronous and less aromatic than those associated with DGT reactions, despite the structural similarities of both types of saddle points.

In order to assess the generality of the results obtained with the model catalysts used above, we have extended our study to the more realistic catalyst *trans*-[Ru-((*R*)-BINAP)(H)(η^2 -

H_2)(*R,R*-dpen)] complex **1c** (BINAP = 2,20-bis-(diphenylphosphino)-1,10-binaphthyl, dpen = 1,2-diphenylethylenediamine) in the reduction of formaldehyde (Scheme 2). Our calculations, which replaced the phenyl groups on *dpen* by methyl groups, indicate that this process occurs concertedly as well through a similar six-membered ring transition structure (TS12, Figure 2) exhibiting synchronicity and aromaticity values ($S_y = 0.73$, NICS(0) = -7.2 ppm) comparable to those found when using the model catalysts **1a** and **1b**. Therefore, these results support the use of the less computationally demanding catalysts **1a,b** in the present study.

One distinct characteristic of the larger catalyst **1c**, however, is its chiral character, which results in two diastereomeric transition states being available for the hydrogenation of the model carbonyl compound acrolein. We have previously described this system in detail,^{3h} but it is worth noticing in this context that the preferred transition state displays significantly more aromatic character (with a NICS comparable to those found for the model catalysts) than the less favored one (see Figure 3). The reduced NICS value for the higher

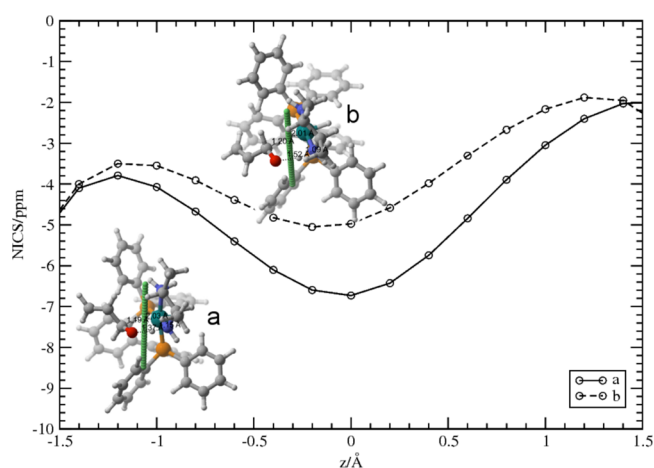


Figure 3. NICS values along an axis perpendicular to the ring formed by the atoms involved in the pericyclic transition state which passes through its center. The values in curve a correspond to the favored transition structure for the hydrogenation of acrolein by catalyst **1c**; those in curve b correspond to the diastereomeric transition state, which was found to be 4.2 kcal/mol higher in energy. These calculations have been performed as described in ref 3h.

energy transition state (4.2 kcal/mol less stable than its alternative) correlates with an also considerably lower value for its synchronicity, which goes from 0.71 to 0.58.

Similar to other in-plane aromatic transition states,¹⁹ the origin of the aromaticity is found in the ring current generated by the six [$\sigma 2s + \sigma 2s + \pi 2s$] electrons involved in the concerted processes which lie approximately in the molecular plane. This current, in turn, promotes a significant diamagnetic shielding at the ring critical point of the electron density leading to the observed negative NICS values. The electronic delocalization within the molecular plane can be viewed with the help of the anisotropy of the induced current density (ACID) method.²¹ As shown in Figure 4a, for the parent transition structure **TS1**, the electronic delocalization is clearly represented by a continuous ring current involving the six atoms which define the molecular plane. Moreover, the current density vectors indicate a diatropic circulation (clockwise vectors) along the molecular plane thus confirming the aromatic nature of this

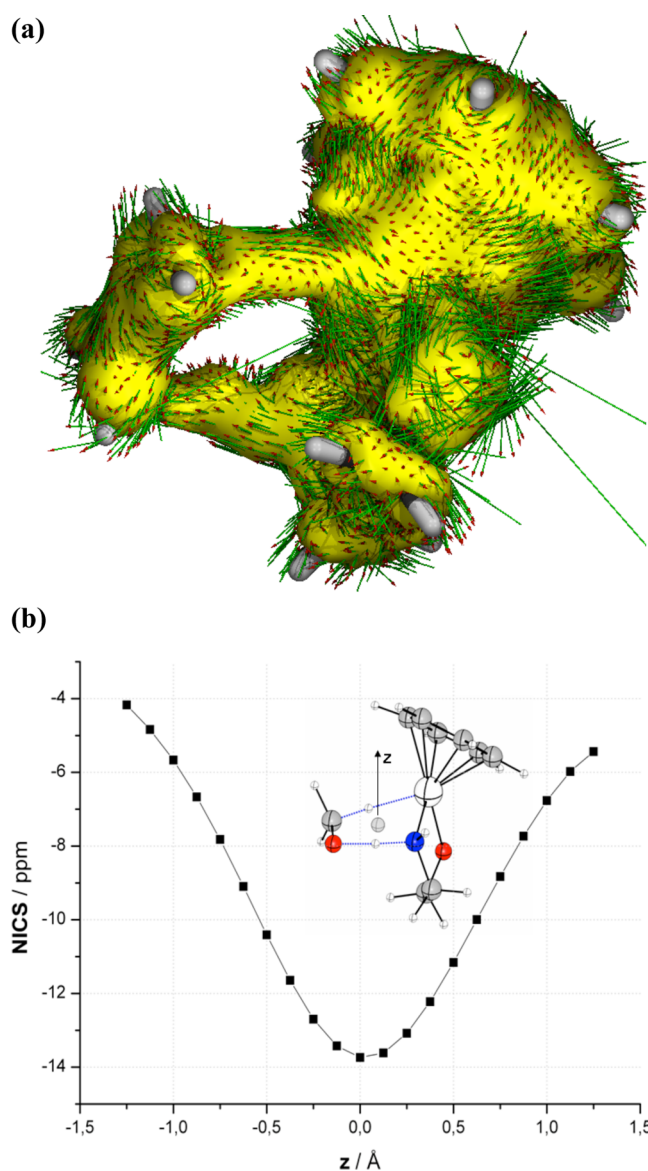


Figure 4. (a) ACID plot of saddle point **TS1** (isosurface value of 0.035 au). (b) Computed NICS values along the z -axis perpendicular to the molecular plane of **TS3**.

kind of transition states. In addition, the variation of the NICS along the z -axis perpendicular to the molecular plane has been also studied for **TS3** to further confirm the in-plane aromatic nature of these species. As expected for this kind of saddle points with in-plane aromaticity,^{6,11} a typical bell-shaped plot with a maximum NICS value at $z = 0$ Å, i.e., in the (3,+1) ring critical point, was found (Figure 4b).

Origins of the Reaction Barriers. From the data in Table 1, it becomes obvious that the hydrogenation reaction proceeds with a lower activation barrier when a heteroatom is involved in the acceptor double bond. The same result is observed when comparing the parent DGT reaction between ethene and ethane versus the MPV reduction of formaldehyde (entries 10 and 11, Table 1). In addition, considering the computed bond lengths in the transition structures of each reaction (Figure 2), there appears to be a correlation between the barrier heights and the geometries of the transition states, in particular, the breaking Ru–H and forming C–H bond distances. In general, it can be observed that shorter forming C–H and longer

breaking Ru–H bond distances are associated with lower reaction barriers. In other words, the transformation seems to be easier for late transition states when the new C–H bond is already developed. This result agrees with kinetic and structural studies in related intramolecular (dyotropic) double hydrogen atom migrations^{5e,f} which indicate that changes of only 0.1–0.17 Å in the initial C···H bond length (also called *precompression factor*) translate into a rate spread of 10^4 s⁻¹.^{5d,30}

A more detailed quantitative insight into the factors controlling the process is given by the activation-strain model. Figure 5 shows the full activation-strain diagrams, i.e.,

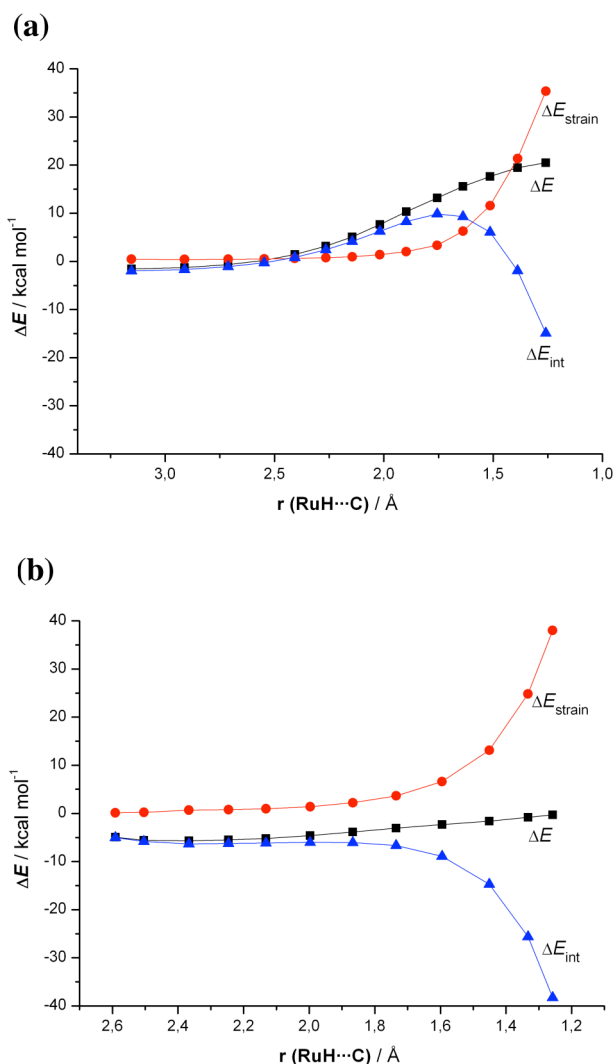


Figure 5. Activation-strain analysis of reactions 6 (a) and 8 (b) along the reaction coordinate projected onto the forming C···H bond distance, computed at the B3LYP/def2-SVP level.

the reaction profile $\Delta E(\zeta)$ together with its decomposition into the strain energy $\Delta E_{\text{strain}}(\zeta)$ and the instantaneous interaction energy $\Delta E_{\text{int}}(\zeta)$ between the deformed reactants, for reactions 6 (reduction of $\text{H}_2\text{C}=\text{CH}_2$ by catalyst **1b**, Figure 5a) and 8 (reduction of $\text{H}_2\text{C}=\text{O}$ by **1b**, Figure 5b).

For the reaction between **1b** and ethene, it can be seen that at the early stages of the process the reaction profile ΔE monotonically becomes more and more destabilized as the reactants approach each other. In the proximity of the transition structure region (i.e., at H···C distances in the

range from 2.0 to 1.5 Å) a sharp increase of ΔE occurs leading to the computed high reaction barrier for this process ($\Delta G_{298}^\ddagger = 28.5$ kcal/mol, see Table 1). Interestingly, at long H···C distances, the interaction energy between the deformed reactants (ΔE_{int}) becomes destabilizing as well contributing to the increase in the total ΔE . This initial increase of ΔE_{int} can be ascribed to steric (Pauli) repulsion between closed shells in the early stages of the reaction as the reactants approach each other. This behavior of ΔE_{int} resembles that found for related DGT reactions¹² and other pericyclic reactions such as [3 + 2] cycloadditions¹⁰ or Alder–ene reactions,¹¹ but it differs from reactions such as $\text{S}_{\text{N}}2$ substitution and E2 elimination^{28a,h} where the net interaction ΔE_{int} is stabilizing along the entire reaction coordinate due to a potent donor–acceptor interaction between the HOMO of the nucleophile/base and the relatively low energy LUMO of the substrate.

If we now further proceed along the reaction coordinate, ΔE_{int} inverts at a certain point, after which this term becomes more and more stabilizing as one approaches the transition structure. This trend agrees with the gain in stability by the above-mentioned aromaticity of the transition state. However, the stabilizing effect of the interaction term cannot compensate the strong destabilizing effect of the deformation energy, ΔE_{strain} ($\Delta E_{\text{int}}^\ddagger = -14.9$ kcal/mol vs $\Delta E_{\text{strain}}^\ddagger = 35.4$ kcal/mol). Therefore, the dominant factor controlling the barrier height of the Noyori reduction of ethene is the energy needed to deform the reactants from their initial equilibrium geometries to the geometries they adopt in the corresponding transition structure.³¹

The situation in the reduction of formaldehyde by the same catalyst **1b** is markedly different (Figure 5b). Here, the interaction does not at first become destabilizing. Thus, it remains nearly constant at long C···H distances and then sharply becomes strongly stabilizing at the vicinity of the transition structure. The stabilization provided by the interaction term ($\Delta E_{\text{int}}^\ddagger = -38.3$ kcal/mol) can now compensate the strain energy and for this reason, this reaction proceeds with a considerable lower reaction barrier ($\Delta G_{298}^\ddagger = 9.4$ kcal/mol, see Table 1). The reason behind this clear stabilization given by ΔE_{int} in the reduction of formaldehyde is of course related to the presence of the heteroatom in the acceptor reactant. Indeed, this is due to the formation of an intramolecular hydrogen-bond between the NH group of the catalyst and the heteroatom which approximates both reactants making the hydrogen transfer much easier. As a consequence of this NH···Y interaction, the ΔE_{int} term does not increase at the beginning of the process and becomes strongly stabilizing at the proximities of the transition structure leading to the observed lower reaction barriers for the processes involving heteroatoms in the initial reactant. Of course, the occurrence of this weak yet important interaction is not possible in those systems lacking heteroatoms (ethene and ethyne), and as a result, the corresponding computed reaction barriers are considerably higher.

CONCLUSIONS

From the results reported in this study, the following conclusions can be drawn: (a) Noyori hydrogenation reactions are processes closely related to double group transfer reactions. Both transformations proceed concertedly via the simultaneous migration of two hydrogen atoms/groups in a pericyclic [$\sigma 2s + \sigma 2s + \pi 2s$] reaction through a six-membered transition structure. (b) Despite that, the former processes are more

asynchronous and the corresponding transition structures less in-plane aromatic. (c) There appears to be a correlation between the barrier heights and the geometries of the transition states, in particular, the breaking Ru–H and forming C–H bond distances. In general, it can be observed that shorter forming C–H and longer breaking Ru–H bond distances are associated with lower reaction barriers. (d) The strain energy associated with the deformation of the initial reactants is the dominant factor controlling the barrier heights of the reactions in the absence of a heteroatom in the acceptor moiety. (e) In contrast, the presence of this heteroatom favors the formation of an intramolecular NH...Y hydrogen bond which approximates both reactants making the hydrogen migration much easier. This is reflected into a strong stabilizing effect of the interaction energy between the reactants which can compensate the destabilizing effect of the strain energy.

■ ASSOCIATED CONTENT

■ Supporting Information

Cartesian coordinates (in Å) and total energies (in au, noncorrected zero-point vibrational energies included) of all stationary points discussed in the text. This material is available free of charge via the Internet at <http://pubs.acs.org>.

■ AUTHOR INFORMATION

Corresponding Author

*E-mail: israel@quim.ucm.es.

Notes

The authors declare no competing financial interest.

■ ACKNOWLEDGMENTS

We are grateful for financial support from the Spanish MINECO and CAM (Grant Nos. CTQ2010-20714-C02-01, CTQ2009-13703, Consolider-Ingenio 2010, CSD2007-00006, S2009/PPQ-1634).

■ REFERENCES

- (1) (a) Noyori, R.; Okhuma, T.; Kitamura, M.; Takaya, H.; Sayo, N.; Kumobayashi, H.; Akuragawa, S. *J. Am. Chem. Soc.* **1987**, *109*, 5856. (b) Noyori, R. *Asymmetric Catalysis in Organic Synthesis*; John Wiley & Sons: New York, 1993; pp 56–82. (c) Ager, D. J.; Laneman, S. A. *Tetrahedron: Asymmetry* **1997**, *8*, 3327. (d) Noyori, R.; Hashiguchi, S. *Acc. Chem. Res.* **1997**, *30*, 97.
- (2) (a) Noyori, R. *Angew. Chem., Int. Ed.* **2002**, *41*, 2008. (b) Knowles, W. S. *Angew. Chem., Int. Ed.* **2002**, *41*, 1998. (c) Noyori, R.; Kitamura, M.; T. Ohkuma, T. *Proc. Natl. Acad. Sci.* **2004**, *101*, 5356.
- (3) Representative examples: (a) Yamakawa, M.; Ito, H.; Noyori, R. *J. Am. Chem. Soc.* **2000**, *122*, 1466. (b) Sandoval, C. A.; Ohkuma, T.; Muñiz, K.; Noyori, R. *J. Am. Chem. Soc.* **2003**, *125*, 13490. (c) Hamilton, R. J.; Leong, C. G.; Bigam, G.; Miskolzie, M.; Bergens, S. H. *J. Am. Chem. Soc.* **2005**, *127*, 4152. (d) Hamilton, R. J.; Bergens, S. H. *J. Am. Chem. Soc.* **2006**, *128*, 13700. (e) Zimmer-De Iulius, M.; Morris, R. H. *J. Am. Chem. Soc.* **2009**, *131*, 11263. (f) Zhang, X.; Guo, X.; Chen, Y.; Tang, Y.; Lei, M.; Fang, W. *Phys. Chem. Chem. Phys.* **2012**, *14*, 6003. (g) Dub, P. A.; Ikariya, T. *J. Am. Chem. Soc.* **2013**, *135*, 2604. (h) Nieto Faza, O.; Fernández, I.; Silva López, C. *Chem. Commun.* **2013**, *49*, 4277.
- (4) Sankararaman, S. *Pericyclic Reactions – A Textbook: Reactions, Applications and Theory*; Wiley: Weinheim, 2005; pp 326–329 and references therein.
- (5) This definition includes textbook reactions like the diimide reduction of double or triple bonds, the Meerwein–Ponndorf–Verley reduction (MPV) of carbonyl groups, and some type II-dyotropic reactions which are characterized by the intramolecular transfer of the two groups (generally hydrogen atoms). See: (a) Reetz, M. T. *Angew. Chem., Int. Ed. Engl.* **1972**, *11*, 130. (b) Reetz, M. T. *Tetrahedron* **1973**, *29*, 2189. (c) Reetz, M. T. *Adv. Organomet. Chem.* **1977**, *16*, 33. (d) Houk, K. N.; Li, Y.; McAllister, M. A.; O'Doherty, G. A.; Paquette, L. A.; Siebrand, W.; Smedarchina, Z. K. *J. Am. Chem. Soc.* **1994**, *116*, 10895. (e) Frenking, G.; Cossío, F. P.; Sierra, M. A.; Fernández, I. *Eur. J. Org. Chem.* **2007**, 5410. (f) Fernández, I.; Cossío, F. P.; Sierra, M. A. *Chem. Rev.* **2009**, *109*, 6687.

- (6) Fernández, I.; Sierra, M. A.; Cossío, F. P. *J. Org. Chem.* **2007**, *72*, 1488.
- (7) Chen, Z.; Wannere, C. S.; Corminboeuf, C.; Puchta, R.; Schleyer, P. v. R. *Chem. Rev.* **2005**, *105*, 3842.
- (8) Bader, R. F. W. *Atoms in Molecules - A Quantum Theory*; Clarendon Press: Oxford, 1990.
- (9) (a) Ess, D. H.; Houk, K. N. *J. Am. Chem. Soc.* **2007**, *129*, 10646. (b) Ess, D. H.; Houk, K. N. *J. Am. Chem. Soc.* **2008**, *130*, 10187. (c) Ess, D. H.; Jones, G. O.; Houk, K. N. *Org. Lett.* **2008**, *10*, 1633. For relevant studies on other pericyclic reactions by the Houk's group, see: (d) Schoenebeck, F.; Ess, D. H.; Jones, G. O.; Houk, K. N. *J. Am. Chem. Soc.* **2009**, *131*, 8121. (e) Xu, L.; Doubleday, C. E.; Houk, K. N. *J. Am. Chem. Soc.* **2010**, *132*, 3029. (f) Krenske, E. H.; Houk, K. N.; Holmes, A. B.; Thompson, J. *Tetrahedron Lett.* **2011**, *52*, 2181.
- (10) Fernández, I.; Cossío, F. P.; Bickelhaupt, F. M. *J. Org. Chem.* **2011**, *76*, 2310.
- (11) Fernández, I.; Bickelhaupt, F. M. *J. Comput. Chem.* **2012**, *33*, 509.
- (12) Fernández, I.; Bickelhaupt, F. M.; Cossío, F. P. *Chem.—Eur. J.* **2009**, *15*, 13022.
- (13) Fernández, I.; Cossío, F. P. *Curr. Org. Chem.* **2010**, *14*, 1578.
- (14) Gaussian 09, Revision B.01: Frisch, M. J.; Trucks, G. W.; Schlegel, H. B.; Scuseria, G. E.; Robb, M. A.; Cheeseman, J. R.; Scalmani, G.; Barone, V.; Mennucci, B.; Petersson, G. A.; Nakatsuji, H.; Caricato, M.; Li, X.; Hratchian, H. P.; Izmaylov, A. F.; Bloino, J.; Zheng, G.; Sonnenberg, J. L.; Hada, M.; Ehara, M.; Toyota, K.; Fukuda, R.; Hasegawa, J.; Ishida, M.; Nakajima, T.; Honda, Y.; Kitao, O.; Nakai, H.; Vreven, T.; Montgomery, J. A., Jr.; Peralta, J. E.; Ogliaro, F.; Bearpark, M.; Heyd, J. J.; Brothers, E.; Kudin, K. N.; Staroverov, V. N.; Kobayashi, R.; Normand, J.; Raghavachari, K.; Rendell, A.; Burant, J. C.; Iyengar, S. S.; Tomasi, J.; Cossi, M.; Rega, N.; Millam, N. J.; Klene, M.; Knox, J. E.; Cross, J. B.; Bakken, V.; Adamo, C.; Jaramillo, J.; Gomperts, R.; Stratmann, R. E.; Yazyev, O.; Austin, A. J.; Cammi, R.; Pomelli, C.; Ochterski, J. W.; Martin, R. L.; Morokuma, K.; Zakrzewski, V. G.; Voth, G. A.; Salvador, P.; Dannenberg, J. J.; Dapprich, S.; Daniels, A. D.; Farkas, Ö.; Foresman, J. B.; Ortiz, J. V.; Cioslowski, J.; Fox, D. J. Gaussian, Inc., Wallingford, CT, 2009.
- (15) (a) Becke, A. D. *Phys. Rev. A* **1988**, *38*, 3098. (b) Lee, C.; Yang, W.; Parr, R. G. *Phys. Rev. B* **1988**, *37*, 785.
- (16) Weigend, F.; Alhrichs, R. *Phys. Chem. Chem. Phys.* **2005**, *7*, 3297.
- (17) González, C.; Schlegel, H. B. *J. Phys. Chem.* **1990**, *94*, 5523.
- (18) Zhao, Y.; Truhlar, D. G. *Acc. Chem. Res.* **2008**, *41*, 157.
- (19) See related examples: (a) Cossío, F. P.; Morao, I.; Jiao, H.; Schleyer, P. v. R. *J. Am. Chem. Soc.* **1999**, *121*, 6737. (b) Fernández, I.; Cossío, F. P.; Sierra, M. A. *Organometallics* **2007**, *26*, 3010. (c) Fernández, I.; Cossío, F. P.; de Cózar, A.; Lledós, A.; Mascareñas, J. L. *Chem.—Eur. J.* **2010**, *16*, 12147. (d) Crespo, O.; Eguillor, B.; Esteruelas, M. A.; Fernández, I.; García-Raboso, J.; Gómez-Gallego, M.; Martín-Ortiz, M.; Oliván, M.; Sierra, M. A. *Chem. Commun.* **2012**, *48*, 5328.
- (20) Wolinski, K.; Hilton, J. F.; Pulay, P. *J. Am. Chem. Soc.* **1990**, *112*, 8251.
- (21) (a) Herges, R.; Geuenich, D. *J. Phys. Chem. A* **2001**, *105*, 3214. (b) Geuenich, D.; Hess, K.; Koehler, F.; Herges, R. *Chem. Rev.* **2005**, *105*, 3758.
- (22) (a) Dewar, M. J. S. *J. Am. Chem. Soc.* **1984**, *106*, 209. (b) Borden, W. T.; Loncharich, R. J.; Houk, K. N. *Annu. Rev. Phys. Chem.* **1988**, *39*, 213.
- (23) Leroy has proposed the term asynchronism in similar contexts. See: Leroy, G.; Sana, M. *Tetrahedron* **1975**, *31*, 2091.

(24) Moyano, A.; Pericás, M. A.; Valentí, E. *J. Org. Chem.* **1989**, *54*, 573.

(25) (a) Lecea, B.; Arrieta, A.; Roa, G.; Ugalde, J. M.; Cossío, F. P. *J. Am. Chem. Soc.* **1994**, *116*, 12314. (b) Lecea, B.; Arrieta, A.; López, X.; Ugalde, J. M.; Cossío, F. P. *J. Am. Chem. Soc.* **1995**, *117*, 12314.

(26) Wiberg, K. B. *Tetrahedron* **1968**, *24*, 1083.

(27) (a) Foster, J. P.; Weinhold, F. *J. Am. Chem. Soc.* **1980**, *102*, 7211.

(b) Reed, A. E.; Weinhold, F. *J. Chem. Phys.* **1985**, *83*, 1736.

(c) Reed, A. E.; Weinstock, R. B.; Weinhold, F. *J. Chem. Phys.* **1985**, *83*, 735. (d) Reed, A. E.; Curtiss, L. A.; Weinhold, F. *Chem. Rev.* **1988**, *88*, 899.

(28) (a) Bickelhaupt, F. M. *J. Comput. Chem.* **1999**, *20*, 114.

(b) Diefenbach, A.; Bickelhaupt, F. M. *J. Chem. Phys.* **2001**, *115*, 4030.

(c) Diefenbach, A.; Bickelhaupt, F. M. *J. Phys. Chem. A* **2004**, *108*,

8460. (d) Diefenbach, A.; de Jong, G. T.; Bickelhaupt, F. M. *J. Chem.*

Theory Comput. **2005**, *1*, 286. (e) van Stralen, J. N. P.; Bickelhaupt, F.

M. *Organometallics* **2006**, *25*, 4260. (f) de Jong, G. T.; Bickelhaupt, F.

M. *ChemPhysChem* **2007**, *8*, 1170. (g) de Jong, G. T.; Bickelhaupt, F.

M. *J. Chem. Theory Comput.* **2007**, *3*, 514. (h) Bento, A. P.;

Bickelhaupt, F. M. *J. Org. Chem.* **2008**, *73*, 7290. (i) Fernández, L.;

Bickelhaupt, F. M.; Cossío, F. P. *Chem.—Eur. J.* **2012**, *18*, 12395.

(j) van Zeist, W.-J.; Bickelhaupt, F. M. *Org. Biomol. Chem.* **2010**, *8*,

3118. (k) Fernández, L.; Solà, M.; Bickelhaupt, F. M. *Chem.—Eur. J.*

2013, DOI: 10.1002/chem.201300648.

(29) Schleyer, P. v. R.; Jiao, H. *Pure Appl. Chem.* **1996**, *68*, 209 and references therein.

(30) Mackenzie, K.; Howard, J. A. K.; Mason, S.; Gravett, E. C.;

Astin, K. B.; Liu, S. X.; Batsanov, A. S.; Vlaovic, D.; Maher, J. P. *J.*

Chem. Soc., Perkin Trans. 2 **1993**, 1211.

(31) The contribution of the individual strain energies of both reactants to the total strain energy is nearly the same (ΔE_{strain} (ethene) = 18.5 kcal/mol vs ΔE_{strain} (**1b**) = 16.8 kcal/mol).